# Production cross sections of $^{47}$Sc via alpha-particle-induced reactions on natural calcium up to 29 MeV

Masayuki Aikawa [a,b,c,*], Yukina Hanada [b], Dagvadorj Ichinkhorloo [a,d], Hiromitsu Haba [e], Sándor Takács [f], Ferenc Ditrói [f], Zoltán Szűcs [f]

[a] *Faculty of Science, Hokkaido University, Sapporo 060-0810, Japan*

[b] *Graduate School of Biomedical Science and Engineering, Hokkaido University, Sapporo 060-8638, Japan*

[c] *Global Center for Biomedical Science and Engineering, Faculty of Medicine, Hokkaido University, Sapporo 060-8648, Japan*

[d] *Nuclear Research Center, National University of Mongolia, Ulaanbaatar 13330, Mongolia*

[e] *Nishina Center for Accelerator-Based Science, RIKEN, Wako 351-0198, Japan*

[f] *Institute for Nuclear Research (ATOMKI), 4026 Debrecen, Hungary*

**Abstract**

Production cross sections of a medical radioisotope $^{47}$Sc via alpha-particle-induced reactions on natural calcium were measured up to 29 MeV. The stacked-foil activation technique and gamma-ray spectrometry were adopted for the experiment. Cross sections of simultaneously formed radionuclides $^{46,44m,44g,43}$Sc and $^{47}$Ca were also determined. Physical yields of the alpha-particle-induced reactions on $^{nat}$Ca and $^{44}$Ca were deduced from the measured cross sections.

**Keyword**

Scandium-47; Calcium target; Alpha-particle irradiation; Cross section; Excitation function

## 1. Introduction

Scandium radionuclides are attractive in the field of medical applications due to their properties and availability, such as $^{43,44}$Sc for PET [1], $^{47}$Sc for therapy [2] and their combination for theranostics [3]. These scandium radionuclides can be produced via charged-particle-induced reactions on calcium, scandium, and titanium [3]. The possible reactions should be investigated in detail in order to optimize the radionuclide production for practical use.

In this paper, we focus on production of $^{47}$Sc ($T_{1/2}$ = 3.3492 d) via alpha-particle-induced reactions on natural calcium, of which isotopic composition is $^{40}$Ca: 96.941%, $^{42}$Ca: 0.647%, $^{43}$Ca: 0.135%, $^{44}$Ca: 2.086%, $^{46}$Ca: 0.004%, and $^{48}$Ca: 0.187% [4]. Among the calcium isotopes, the alpha-particle-induced reactions on $^{44}$Ca, $^{46}$Ca, and $^{48}$Ca can provide $^{47}$Sc, and its parent $^{47}$Ca ($T_{1/2}$ = 4.536 d) and grandparent $^{47}$K ($T_{1/2}$ = 17.50 s). Taking into account the relatively small abundance of $^{46}$Ca and $^{48}$Ca, the most probable reaction for

* Corresponding author: Masayuki AIKAWA (aikawa@sci.hokudai.ac.jp), Faculty of Science, Hokkaido University, Sapporo 060-0810, Japan

production of $^{47}$Sc in a larger quantity is the $^{44}$Ca(α,p)$^{47}$Sc reaction. We found only one experimental study for the $^{47}$Sc production [5] in a literature survey and the related data in the EXFOR library [6]. Therefore, we performed an experiment to obtain cross sections of the $^{nat}$Ca(α,x)$^{47}$Sc reaction up to 29 MeV. The cross sections on $^{nat}$Ca can be normalized to those on enriched $^{44}$Ca under assumption of negligible contributions from $^{46}$Ca and $^{48}$Ca. In addition, production cross sections of $^{46,44m,44g,43}$Sc and $^{47}$Ca were measured to estimate the amount of the co-produced radioactive impurities. The physical yields of the alpha-particle-induced reactions on $^{nat}$Ca and $^{44}$Ca were deduced from the measured cross sections.

## 2. Experimental details and data analysis

The experiment was conducted with a 29-MeV alpha-particle beam at the AVF cyclotron in RIKEN. The stacked-foil activation technique and high-resolution off-line gamma-ray spectrometry were adopted in the measurement.

Calcium-fluoride ($CaF_2$) was used as a target material. The stacked target consisted of thin $CaF_2$ layers, two types of Al foils ($Al_H$, purity: 99.999%, thickness: 10 μm, size: 100 × 100 mm, Goodfellow Cambridge Ltd., UK and $Al_L$, purity: >99%, thickness: 5 μm, size: 100 × 100 mm, The Nilaco Corporation, Japan) and $^{nat}$Ti foil (purity: 99.5%, thickness: 5 μm, size: 50 × 100 mm, The Nilaco Corporation, Japan). By measuring the lateral size and mass of the purchased Al and Ti foils, their average thicknesses were determined for the data analysis. The measured thicknesses of $Al_H$, $Al_L$ and $^{nat}$Ti foils were 2.57, 1.50 and 2.30 mg/cm$^2$, respectively. The $^{nat}$Ti foil was used for monitoring the beam parameters by using the $^{nat}$Ti(α,x)$^{51}$Cr monitor reaction and to check the energy loss of the alpha-particles through the stacked target. The $Al_L$ foil was used to catch the recoiled reaction products from the $^{nat}$Ti foil in the stack. The $Al_H$ foil was used as a backing of the $CaF_2$ layer. The $CaF_2$ layer was deposited on the $Al_H$ foil using a vacuum evaporation method. The thickness of the $CaF_2$ layer was determined to be 0.135 mg/cm$^2$ from the deposited area (90 × 90 mm) and weight of $CaF_2$. All foils were cut into 10 × 10 mm pieces to construct the stacked target and to fit a target holder served as a Faraday cup. The $CaF_2$ layers were sandwiched with the $Al_H$ foils as $Al_H(CaF_2)$-$(CaF_2)Al_H$ to collect the recoiled reaction products from the thin $CaF_2$ layer and to increase the target thickness. Twelve sets of the $Al_H(CaF_2)$-$(CaF_2)Al_H$ foils and seven sets of the $^{nat}$Ti-$Al_L$ foils were stacked together in the target holder. The configuration of the stacked target is listed in Table 1.

The stacked target was irradiated for 30 min with an alpha-particle beam collimated to 3 mm in diameter. The average beam intensity measured by charge integration on the Faraday cup was 175 nA. The primary beam energy measured using the time-of-flight (TOF) method [7] was 29.0±0.2 MeV. Energy degradation in the stacked target was calculated using stopping powers obtained from the SRIM code [8]. The calculation of the energy degradation was checked by using the $^{nat}$Ti(α,x)$^{51}$Cr monitor reaction.

The high-resolution gamma-ray spectrometry of the activated foils was done without chemical separation. A high-purity germanium detector (ORTEC GEM30P4-70) and a dedicated software (SEIKO EG&G Gamma Studio) were used for the gamma-ray measurement and spectrum analysis. The efficiency of the detector was calibrated with a multiple gamma-ray emitting point-like source (Eckert & Ziegler Isotope Products). The point-like source consisted of eight radionuclides, $^{57,60}$Co, $^{88}$Y, $^{109}$Cd, $^{113}$Sn $^{137}$Cs, $^{139}$Ce and $^{241}$Am to cover the energy range between 60 and 1836 keV. Gamma rays emitted from each activated foil were measured using the energy- and geometry-dependent, and efficiency-calibrated detector. Each set of the $Al_H(CaF_2)$-$(CaF_2)Al_H$ foils was measured 5 times with cooling times from 3.2 h to 77.0 d. The associated dead times were kept below 2.1%. The experimental parameters are summarized in Table 2. Nuclear data required to determine cross sections collected in Table 3 were retrieved from the online databases, NuDat 2.8 [9], LiveChart [10], Lund/LBNL Nuclear Data Search [11], and QCalc [12].

Cross sections $\sigma$ were deduced using the following activation formula

$$\sigma = \frac{N_\gamma \lambda}{\varepsilon_d \varepsilon_\gamma \varepsilon_t N_t N_b (1 - e^{-\lambda t_b}) e^{-\lambda t_c} (1 - e^{-\lambda t_m})} \quad (1)$$

where $N_\gamma$ is the measured net count of the peak area, $\lambda$ is the decay constant ($s^{-1}$), $\varepsilon_d$ is the detector efficiency, $\varepsilon_\gamma$ is the gamma-ray intensity, $\varepsilon_t$ is the dead time correction, $N_t$ is the surface density of target atoms ($cm^{-2}$), $N_b$ is the number of projectiles per unit time ($s^{-1}$), $t_b$ is the irradiation time (s), $t_c$ is the cooling time (s), and $t_m$ is the acquisition time (s).

Cross sections of the $^{nat}Ti(\alpha,x)^{51}Cr$ monitor reaction were derived to assess the beam parameters and the target thicknesses. The gamma line at 320.08 keV ($I_\gamma$ = 9.91%) emitted from each pair of the $^{nat}Ti$-$Al_L$ foils was measured. Recoiled products from the $^{nat}Ti$ foils were caught by the next $Al_L$ foils. The cross sections derived using the spectra with dead times less than 0.6% were compared with the IAEA recommended values [13]. According to the comparison, the beam intensity was corrected by +5.6% to have agreement with the amplitude of the measured and recommended values. The corrected beam intensity 185 nA was accepted and used in the data analysis. The peak position was found to be slightly shifted to the lower energy side. As the beam energy was measured by the TOF method the primary beam energy was accepted and the energy loss of the alpha particle in the stack was adjusted by changing the thicknesses of the $Al_H$ and $Al_L$ foils in the stack by -1% within the uncertainty of the given foil thicknesses. The measured thicknesses of the $^{nat}Ti$ foil and the $CaF_2$ layer were adopted without any correction. The cross sections using the corrected parameters agree with the recommended values as shown in Fig. 1. The adopted parameters for deduction of cross sections are also listed in Table 2.

Table 1. Configuration of the stacked target. The $CaF_2$ layers were sandwiched with the $Al_H$ foils.

| No. | Foil/(Layer) | No. | Foil/(Layer) | No. | Foil/(Layer) | No. | Foil/(Layer) |
|---|---|---|---|---|---|---|---|
| 1 | $Al_H$<br>($CaF_2$) | 9<br>10 | Ti<br>$Al_L$ | 19 | $Al_H$<br>($CaF_2$) | 29<br>30 | Ti<br>$Al_L$ |
| 2 | ($CaF_2$)<br>$Al_H$ | 11 | $Al_H$<br>($CaF_2$) | 20 | ($CaF_2$)<br>$Al_H$ | 31 | $Al_H$<br>($CaF_2$) |
| 3 | $Al_H$<br>($CaF_2$) | 12 | ($CaF_2$)<br>$Al_H$ | 21<br>22 | Ti<br>$Al_L$ | 32 | ($CaF_2$)<br>$Al_H$ |
| 4 | ($CaF_2$)<br>$Al_H$ | 13 | $Al_H$<br>($CaF_2$) | 23 | $Al_H$<br>($CaF_2$) | 33<br>34 | Ti<br>$Al_L$ |
| 5 | $Al_H$<br>($CaF_2$) | 14 | ($CaF_2$)<br>$Al_H$ | 24 | ($CaF_2$)<br>$Al_H$ | 35 | $Al_H$<br>($CaF_2$) |
| 6 | ($CaF_2$)<br>$Al_H$ | 15<br>16 | Ti<br>$Al_L$ | 25<br>26 | Ti<br>$Al_L$ | 36 | ($CaF_2$)<br>$Al_H$ |
| 7 | $Al_H$<br>($CaF_2$) | 17 | $Al_H$<br>($CaF_2$) | 27 | $Al_H$<br>($CaF_2$) | 37<br>38 | Ti<br>$Al_L$ |
| 8 | ($CaF_2$)<br>$Al_H$ | 18 | ($CaF_2$)<br>$Al_H$ | 28 | ($CaF_2$)<br>$Al_H$ | | |

Table 2. Experimental parameters.

| | |
|---|---|
| **Target** | |
| Measured (corrected) thickness (mg/cm$^2$) | $CaF_2$: 0.135 |
| | $^{27}$Al ($Al_H$, purity: 99.999%): 2.57 (2.55) |
| | $^{27}$Al ($Al_L$, purity: >99%): 1.50 (1.49) |
| | $^{nat}$Ti: 2.30 |
| Stack composition | 12 sets of $Al_H$($CaF_2$)-($CaF_2$)$Al_H$ foils |
| | 7 sets of $^{nat}$Ti-$Al_L$ foils |
| **Beam** | |
| Measured (corrected) beam current (nA) | 175 (185) ±11 |
| Primary energy (MeV) | 29.0 ±0.2 |
| Irradiation period (min) | 30.0 |
| **Measurement** | |
| Series: Cooling time (distance, dead time) | Ser. 1: 3.2-5.4 h (10 cm, 0.8-1.9%) |
| | Ser. 2: 5.6-21.6 h (5 cm, 0.1-1.8%) |
| | Ser. 3: 1.2-2.8 d (1 cm, 0.1%) |
| | Ser. 4: 2.9-3.0 d (1 cm, <0.1%) |
| | Ser. 5: 43.5-77.0 d (1 cm, <0.1%) |

Table 3. Reaction and decay data retrieved from online databases [9–12].

| Nuclide | Half-life | Decay mode (%) | $E_\gamma$ (keV) | $I_\gamma$ (%) | Contributing reaction | Q-value (MeV) | Threshold energy (MeV) |
|---|---|---|---|---|---|---|---|
| $^{47}$Sc | 3.3492 d | $\beta^-$ (100) | **159.381** | **68.3(4)** | $^{44}$Ca(α,p) | -2.0 | 2.2 |
| | | | | | $^{46}$Ca(α,t) | -11.3 | 12.3 |
| | | | | | $^{48}$Ca(α,t2n) | -28.6 | 30.9 |
| | | | | | $^{47}$Ca decay | | |
| $^{46}$Sc | 83.79 d | $\beta^-$ (100) | **889.277** | **99.9840(10)** | $^{43}$Ca(α,p) | -1.5 | 1.7 |
| | | | 1120.545 | 99.9870(10) | $^{44}$Ca(α,d) | -10.4 | 11.4 |
| | | | | | $^{46}$Ca(α,tn) | -22.0 | 23.9 |
| $^{44m}$Sc | 58.61 h | ε+$\beta^+$ (1.20) | **271.241** | **86.74(6)** | $^{42}$Ca(α,d) | -11.7 | 12.8 |
| | | IT (98.80) | | | $^{43}$Ca(α,t) | -13.4 | 14.6 |
| | | | | | $^{44}$Ca(α,tn) | -24.5 | 26.7 |
| $^{44g}$Sc | 3.97 h | ε+$\beta^+$ (100) | 511.0 | 188.54(10) | $^{42}$Ca(α,d) | -11.4 | 12.5 |
| | | | **1157.020** | **99.9(4)** | $^{43}$Ca(α,t) | -13.1 | 14.3 |
| | | | | | $^{44}$Ca(α,tn) | -24.2 | 26.5 |
| | | | | | $^{44}$Ti decay | | |
| $^{43}$Sc | 3.891 h | ε+$\beta^+$ (100) | **372.9** | **22.5(7)** | $^{40}$Ca(α,p) | -3.5 | 3.9 |
| | | | 511.0 | 176.2(16) | $^{42}$Ca(α,t) | -14.9 | 16.3 |
| | | | | | $^{43}$Ca(α,tn) | -22.8 | 24.9 |
| | | | | | $^{40}$Ca(α,n)$^{43}$Ti decay | -11.2 | 12.3 |
| $^{47}$Ca | 4.536 d | $\beta^-$ (100) | **1297.09** | **67(13)** | $^{46}$Ca(α,$^{3}$He) | -13.3 | 14.5 |
| | | | | | $^{48}$Ca(α,αn) | -10.0 | 10.8 |
| | | | | | $^{48}$Ca(α,αp)$^{47}$K decay | -15.8 | 17.1 |
| $^{51}$Cr | 27.704 d | ε (100) | **320.0824** | **9.910(10)** | | | |

Gamma lines in bold were used for data evaluation.

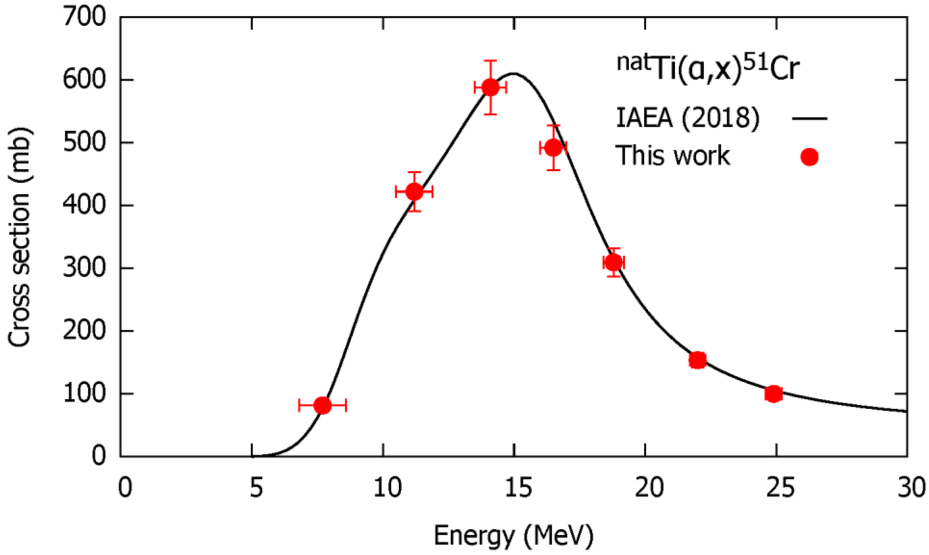

Fig. 1. Excitation function of the $^{nat}Ti(\alpha,x)^{51}Cr$ monitor reaction with the IAEA recommended values [13].

## 3. Results and discussion

The production cross sections of $^{47,46,44m,44g,43}Sc$ and $^{47}Ca$ via the alpha-particle-induced reactions measured on CaF2 targets up to 29 MeV were converted to those on natural calcium targets. The derived cross sections are summarized in Table 4. The results are graphically shown in Figs. 2-7 with experimental data in the literature [5,14,15] and the model based theoretical cross sections available in the TENDL-2019 library [16]. The cross sections on the enriched targets [5,15] were normalized to those of natural targets using the isotopic ratios of natural calcium. Physical yields of $^{47}Sc$ in the alpha-particle-induced reactions on $^{nat}Ca$ and the enriched $^{44}Ca$ were deduced using the measured cross sections and are shown in Fig. 8.

The median projectile energies in each sandwiched pair of the $CaF_2$ layers are listed in Table 4. The total energy uncertainties of 0.2-0.8 MeV were propagated from the uncertainties of the primary beam energy (0.2 MeV) and the target thicknesses (1-5%). The total uncertainties of 9.3-35.1% for the cross sections are calculated from the square roots of the quadratic summation of the linearly propagated components. The components taken into account are beam intensity (6%), gamma-ray intensity (<19.4%), detector efficiency (5%), target thickness (5%) and counting statistics (0.3-27.8%).

Table 4. Production cross sections via the alpha-particle-induced reactions on natural calcium.

| Energy (MeV) | $^{47}$Sc (mb) | $^{46}$Sc (mb) | $^{44m}$Sc (mb) | $^{44g}$Sc (mb) | $^{43}$Sc (mb) | $^{47}$Ca (mb) |
|---|---|---|---|---|---|---|
| 28.6 ±0.2 | 0.486 ±0.048 | 7.47 ±1.02 | 3.33 ±0.31 | 1.67 ±0.18 | 53.9 ±5.4 | 0.0724 ±0.0254 |
| 27.6 ±0.2 | 0.530 ±0.069 | 7.70 ±0.94 | 3.27 ±0.31 | 1.75 ±0.19 | 66.9 ±6.6 | |
| 26.6 ±0.2 | 0.562 ±0.061 | 7.32 ±0.99 | 3.13 ±0.30 | 1.74 ±0.19 | 81.8 ±8.1 | |
| 25.6 ±0.2 | 0.636 ±0.069 | 6.78 ±0.91 | 3.03 ±0.29 | 1.87 ±0.20 | 97.9 ±9.7 | |
| 23.9 ±0.3 | 0.902 ±0.092 | 6.09 ±0.74 | 2.76 ±0.26 | 1.47 ±0.17 | 150 ±15 | |
| 22.8 ±0.3 | 1.18 ±0.12 | 5.63 ±0.72 | 2.63 ±0.25 | 1.36 ±0.16 | 193 ±19 | |
| 20.9 ±0.3 | 1.67 ±0.16 | 4.56 ±0.67 | 1.74 ±0.17 | 0.906 ±0.108 | 292 ±29 | |
| 19.6 ±0.4 | 2.13 ±0.20 | 3.33 ±0.48 | 1.03 ±0.10 | 0.588 ±0.082 | 371 ±36 | |
| 17.5 ±0.4 | 2.82 ±0.27 | 1.91 ±0.49 | 0.142 ±0.023 | 0.116 ±0.031 | 516 ±51 | |
| 15.1 ±0.5 | 2.57 ±0.25 | | | | 557 ±55 | |
| 12.5 ±0.6 | 1.64 ±0.16 | | | | 478 ±47 | |
| 9.3 ±0.8 | 0.752 ±0.078 | | | | 232 ±23 | |

### 3.1 The $^{nat}Ca(\alpha,x)^{47}Sc$ reaction

$^{47}Sc$ ($T_{1/2}$ = 3.3492 d) can be produced from three stable isotopes of calcium. The main contribution is expected to be the direct $^{44}Ca(\alpha,p)^{47}Sc$ reaction. $^{47}Sc$ can also be formed by decay of the co-produced $^{47}Ca$ ($T_{1/2}$ = 4.536 d) and $^{47}K$ ($T_{1/2}$ = 17.50 s). $^{47}Ca$ can be formed in the alpha-particle-induced reactions on two calcium isotopes ($^{46}Ca$: 0.004% and $^{48}Ca$: 0.187%), while $^{47}K$ can be formed only on $^{48}Ca$. The gamma line at 159.381 keV ($I_\gamma$ = 68.3%) followed by the decay of $^{47}Sc$ was measured after cooling times of 1.2-2.8 d (Ser. 3). Their contributions from the two parent radionuclides were expected to be small because of the very low abundances of the two target isotopes. The measured cross section for $^{47}Ca$ production is only 0.0765 mb at 28.6 MeV (see section 3.6). No experimental information is available for the $^{48}Ca(\alpha,\alpha p)^{47}K$ reaction, but according to the TENDL-2019 database the predicted cross sections are in the range of micro barn at a 30 MeV alpha-particle energy.

The cross sections of the $^{nat}Ca(\alpha,x)^{47}Sc$ reaction were derived and shown in Fig. 2 in comparison with the previous experimental data [5] and the theoretical values in the TENDL-2019 library [16]. The previous data of the $^{44}Ca(\alpha,p)^{47}Sc$ reaction are normalized using the isotopic ratio of natural calcium. The peak position of the previous study is slightly shifted to the lower energy than that of ours. The previous data are larger below 15 MeV and smaller between 15 and 20 MeV than ours. The theoretically calculated values in the TENDL-2019 library overestimates both experimental results by a factor of 2 around at the peak energy.

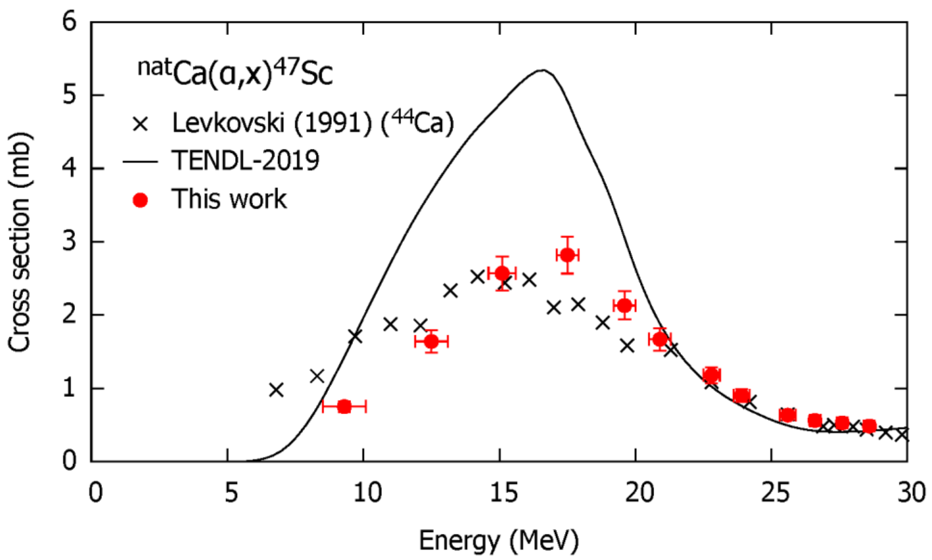


Fig. 2. Cross sections of the $^{nat}Ca(\alpha,x)^{47}Sc$ reaction with the normalized values from the previous data [5] and the theoretical values from the TENDL-2019 library [16].

### 3.2 The $^{nat}Ca(\alpha,x)^{46}Sc$ reaction

The radionuclide $^{46}Sc$ can be produced in the alpha-particle-induced reactions on the $^{43,44,46,48}Ca$ target isotopes. However, contribution from the reactions on $^{48}Ca$ is not possible in the energy range of this work. $^{46}Sc$ has two isomeric states, the ground state $^{46g}Sc$ ($T_{1/2}$ = 83.79 d) and the short-lived meta-stable state $^{46m}Sc$ ($T_{1/2}$ = 18.75 s) decaying 100% to the ground state by the IT decay mode. The co-produced isomer $^{46m}Sc$ completely decayed to the ground state before the measurement started. The cross sections of the $^{nat}Ca(\alpha,x)^{46g+m}Sc$ reaction were determined using the gamma line at 889.277 keV ($I_\gamma$ = 99.9840%). The spectra collected after cooling times of 43.5-77.0 d (Ser. 5) were used to determine the cross sections. The derived cross sections are compared with the previous experimental data [5] and the theoretically calculated values in the TENDL-2019 library [16] as shown in Fig. 3. The experimental data on the enriched targets of $^{43}Ca$ and $^{44}Ca$ in the previous study [3] were normalized using the isotopic ratio of natural calcium. The dominant contribution comes from $^{44}Ca$ due to approximately 15 times larger abundance of $^{44}Ca$ than $^{43}Ca$. The normalized values for the $^{44}Ca(\alpha,x)^{46}Sc$ reaction in the previous study are slightly larger than ours below 25 MeV (see Fig 3.). The theoretical values of the TENDL-2019 library overestimates both experimental results above 20 MeV.

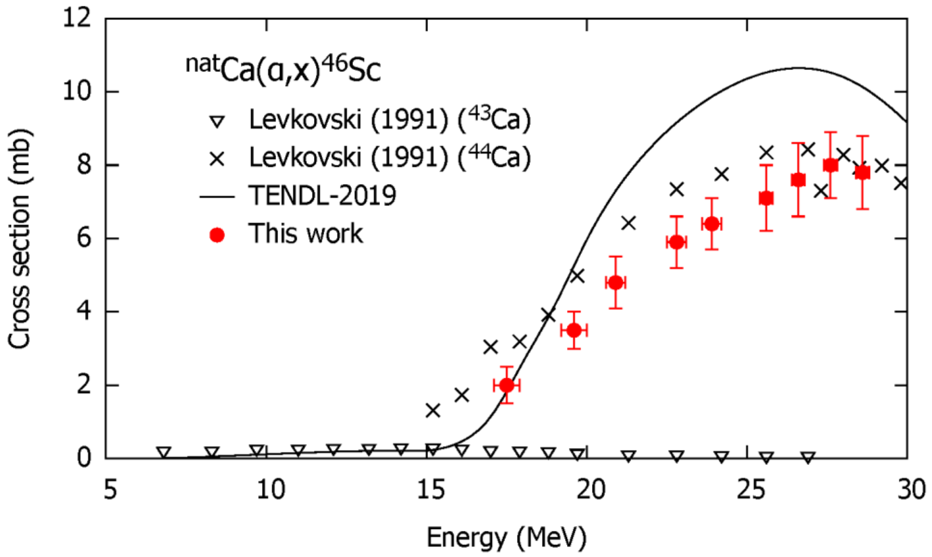


Fig. 3. Cross sections of the $^{nat}Ca(\alpha,x)^{46}Sc$ reaction with the normalized values from the previous data [5] and the theoretical values from the TENDL-2019 library [16].

### 3.3 The $^{nat}Ca(\alpha,x)^{44m}Sc$ reaction

Contribution for the formation of $^{44m}Sc$ ($T_{1/2}$ = 58.61 h) is possible from $^{42,42,44}Ca$ up to 30-MeV alpha-particle energy. The gamma line at 271.241 keV ($I_\gamma$ = 86.74%) following the decay of $^{44m}Sc$ was used to assess the activity of the activated target foils. The spectra measured after cooling times of 1.2-2.8 d (Ser. 3) were adopted for cross section determination. The measured cross sections of the $^{nat}Ca(\alpha,x)^{44m}Sc$ reaction are shown in Fig. 4, in which the results are compared with the previous experimental data [5] and the theoretical predication in the TENDL-2019 library [16]. The previous data on the enriched targets of $^{42}Ca$ and $^{43}Ca$ were normalized using the isotopic ratio of natural calcium. The normalized values from the $^{42}Ca$ target agree with our results above 23 MeV, however the literature data below 20 MeV are higher than our deduced cross sections. The theoretical prediction in the TENDL-2019 library is almost consistent with our data below 25 MeV, but is lower than ours at the higher energies.

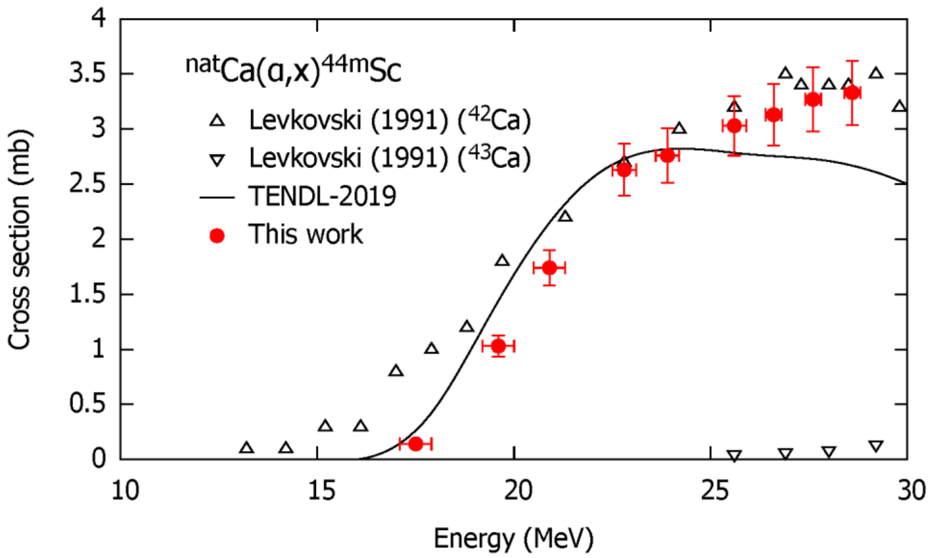


Fig. 4. Cross sections of the $^{nat}Ca(\alpha,x)^{44m}Sc$ reaction with the normalized values from the previous data [5] and the theoretical values from the TENDL-2019 library [16].

**3.4 The $^{nat}Ca(\alpha,x)^{44g}Sc$ reaction**

Beside the direct production of $^{44g}Sc$ ($T_{1/2}$ = 3.97 h) it can be populated by decay of the much longer-lived $^{44m}Sc$ ($T_{1/2}$ = 58.61 h) and $^{44}Ti$ ($T_{1/2}$ = 59.1 y). The gamma line at 1157.020 keV ($I_\gamma$ = 99.9%) from the decay of $^{44g}Sc$ ($T_{1/2}$ = 3.97 h) was used to assess the activity of the target foils. The spectra including the partial contribution of $^{44m}Sc$ were measured after cooling times of 5.6-21.6 h (Ser. 2). To subtract the contribution of $^{44m}Sc$ from the measured net counts, the activities of $^{44g}Sc$ ($A_g$) and $^{44m}Sc$ ($A_m$) at the end-of-bombardment were calculated using the cross sections ($\sigma_m$) derived in section 3.3 as:

$$A_g = N_t N_b \sigma_g \left(1 - e^{-\lambda_g t_b}\right) + \varepsilon_{IT} N_t N_b \sigma_m \frac{\lambda_g \lambda_m}{\left(\lambda_g - \lambda_m\right)} \left( \frac{\left(1 - e^{-\lambda_m t_b}\right)}{\lambda_m} - \frac{\left(1 - e^{-\lambda_g t_b}\right)}{\lambda_g} \right) \quad (2)$$

$$A_m = N_t N_b \sigma_m \left(1 - e^{-\lambda_m t_b}\right) \quad (3)$$

where $\sigma_g$ is the cross section for $^{44g}Sc$, $\lambda_g$ and $\lambda_m$ are the decay constants of $^{44g}Sc$ and $^{44m}Sc$ ($s^{-1}$), $\varepsilon_{IT}$ is the decay branching ratio (IT: 98.8%) from $^{44m}Sc$ to $^{44g}Sc$. The expected net count of the gamma line $N_\gamma$ was:

$$N_\gamma = \varepsilon_d \varepsilon_\gamma \varepsilon_t \left( A_g \frac{e^{-\lambda_g t_c}\left(1 - e^{-\lambda_g t_m}\right)}{\lambda_g} + \varepsilon_{IT} A_m \frac{\lambda_g}{(\lambda_g - \lambda_m)} \left( \frac{e^{-\lambda_m t_c}\left(1 - e^{-\lambda_m t_m}\right)}{\lambda_m} - \frac{e^{-\lambda_g t_c}\left(1 - e^{-\lambda_g t_m}\right)}{\lambda_g} \right) \right). \quad (4)$$

From Eqs. (2)-(4) and the measured net counts, we could determine $\sigma_g$. The contribution of $^{44}Ti$ was negligibly small due to its long half-life ($T_{1/2}$ = 59.1 y) and no peaks at 67.87 ($I_\gamma$ = 93.0%) and 78.32 keV ($I_\gamma$ = 96.4%) from the decay of $^{44}Ti$ were found in any measured spectra.

The independent cross sections of the $^{nat}Ca(\alpha,x)^{44g}Sc$ reaction are thus determined and shown in Fig. 5 in comparison with the previous experimental data [5] and the theoretical predication in the TENDL-2019 library [16]. The previous data on the enriched targets of $^{42}Ca$ and $^{43}Ca$ were normalized using the isotopic ratio of natural calcium. The normalized values of Levkovski (1991) for the $^{42}Ca(\alpha,x)^{44g}Sc$ reaction alone (not including the contribution of the $^{43}Ca(\alpha,x)^{44g}Sc$ reaction) are slightly larger than our measured cross sections. The prediction of the model based theoretical values in the TENDL-2019 library agrees well with our result.

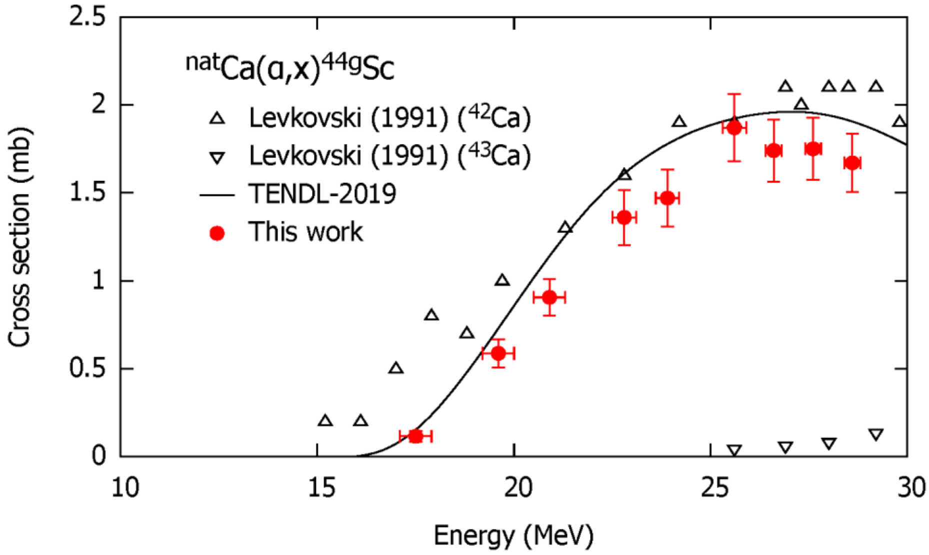

Fig. 5. Cross sections of the $^{nat}Ca(\alpha,x)^{44g}Sc$ reaction with the normalized values from the previous data [5] and the theoretical values from the TENDL-2019 library [16].

### 3.5 The $^{nat}Ca(\alpha,x)^{43}Sc$ reaction

Reactions on the $^{40,42,43}Ca$ target isotopes can contribute to the direct formation of $^{43}Sc$ ($T_{1/2}$ = 3.891 h) in the investigated energy range. Decay of co-produced $^{43}Ti$ ($T_{1/2}$ = 509 ms) may also provide considerable contribution as the $^{40}Ca(\alpha,n)^{43}Ti$ reaction takes place on the most abundant $^{40}Ca$ (96.941%) isotope. To assess the $^{nat}Ca(\alpha,x)^{43}Sc$ process the gamma line at 372.9 keV ($I_\gamma$ = 22.5%) from decay of $^{43}Sc$ was used. Spectra collected after cooling times of 5.6-21.6 h (Ser. 2) were used. The applied cooling times assured complete decay of the co-produced $^{43}Ti$ to $^{43}Sc$. The cumulative cross sections of the $^{nat}Ca(\alpha,x)^{43}Sc$ reaction were derived. The result shown in Fig. 6 is compared with the previous experimental data [5,14,15] and the theoretical predication in the TENDL-2019 library [16]. The previous data of the $^{40}Ca(\alpha,p)^{43}Sc$ reaction [5,15] are normalized using the isotopic ratio of natural calcium. The two experimental datasets by Levkovski (1991) and Alabyad et al. (2018) agree with our data above 12 MeV within uncertainties. Their data at the lower energy region below 12 MeV are larger than ours. The data by Howard et al. (1974) show similar shape but higher amplitude above 10 MeV. The peak position of the TENDL-2019 values is almost consistent with the experimental data, although the peak amplitude is higher than our data.

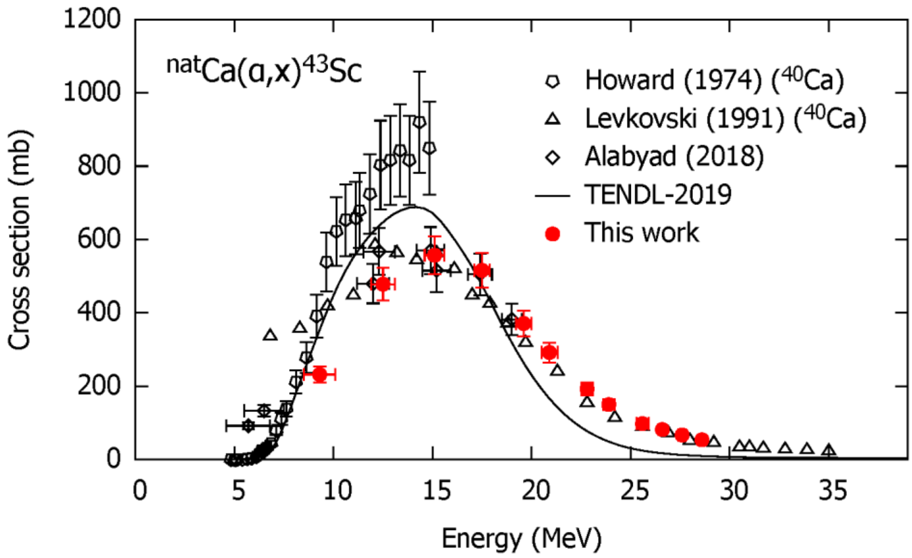


Fig. 6. Cross sections of the $^{nat}Ca(\alpha,x)^{43}Sc$ reaction with the previous data [14], the normalized values from the previous data [5,15] and the theoretical values from the TENDL-2019 library [16].

### 3.6 The $^{nat}Ca(\alpha,x)^{47}Ca$ reaction

Since $^{47}Ca$ can be produced only in the reactions from the low abundant $^{46,48}Ca$ target isotopes, the expected cross section is low. The cross sections of the $^{nat}Ca(\alpha,x)^{47}Ca$ reaction were determined using the gamma line at 1297.09 keV ($I_\gamma$ = 67%) from decay of $^{47}Ca$ ($T_{1/2}$ = 4.536 d). Decay contribution from the energetically possible co-produced parent $^{47}K$ ($T_{1/2}$ = 17.50 s), which completely decayed to $^{47}Ca$ during the cooling times of 1.2-2.8 d (Ser. 3), is also included. Therefore, the deduced cross section is considered to be cumulative. Only one cross section of the $^{nat}Ca(\alpha,x)^{47}Ca$ reaction was deduced at the highest bombarding particle energy of 28.6 MeV with a statistical uncertainty below 30%. Due to the large relative uncertainty (19.4%) of the gamma-ray intensity and the poor counting statistics (27.8%), the cross section has a large total relative uncertainty of 35.0%. The result is shown in Fig. 7 and compared with the theoretical predication in the TENDL-2019 library [16]. The TENDL-2019 predicted value is a factor of two higher than our experimental data. No experimental data were found in the literature for this reaction.

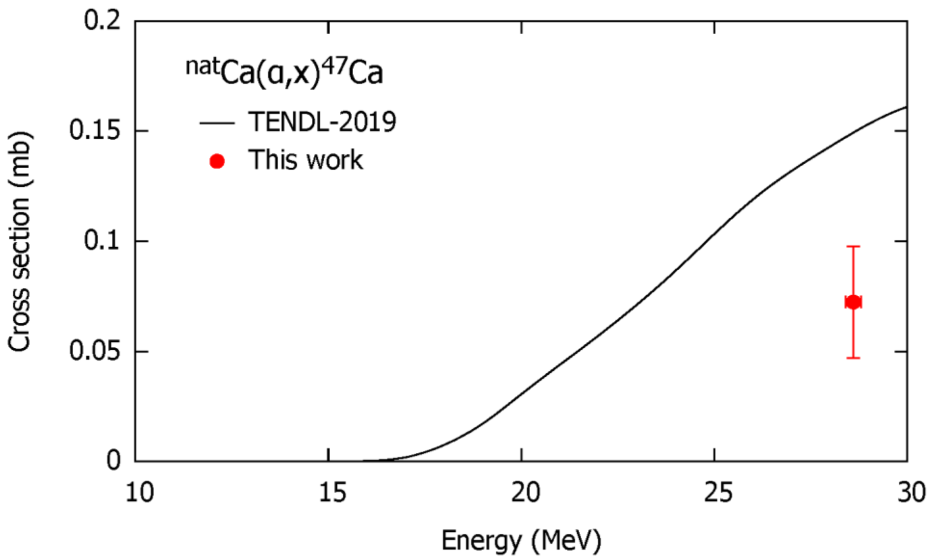


Fig. 7. Cross sections of the $^{nat}Ca(\alpha,x)^{47}Ca$ reaction with the theoretical values from the TENDL-2019 library [16].

### 3.7 Physical yield of $^{47}$Sc

Physical yields [17] for production of $^{47}$Sc in the alpha-particle-induced reactions on $^{nat}$Ca and the enriched $^{44}$Ca were deduced from the measured cross sections of the $^{nat}$Ca(α,x)$^{47}$Sc reaction presented in section 3.1. Assuming that the contributions from reactions on low abundant target isotopes $^{46,48}$Ca were negligibly small, the yield was transformed to a 100% $^{44}$Ca target. The deduced physical yields using $^{nat}$Ca and $^{44}$Ca can reach 34.5 and 1650 kBq/μAh at 20 MeV, respectively. Above 20 MeV, the amount of the longer-lived $^{46}$Sc impurity is getting too high. For practical use of $^{47}$Sc, the amount of the co-produced longer-lived impurity of $^{46}$Sc should be estimated. The reaction threshold energy of the $^{44}$Ca(α,d)$^{46}$Sc reaction is $E_{th}$ = 11.4 MeV. However, the lowest energy cross section point measured by us for the $^{nat}$Ca(α,d)$^{46}$Sc reaction is 17.5 MeV. Therefore, the experimental data were extended down to the threshold energy of the reaction by using the TENDL-2019 prediction. Using this assumption, the estimated yields of the co-produced $^{46}$Sc impurity using the $^{nat}$Ca and $^{44}$Ca targets are 0.74 and 35.5 kBq/μAh, respectively.

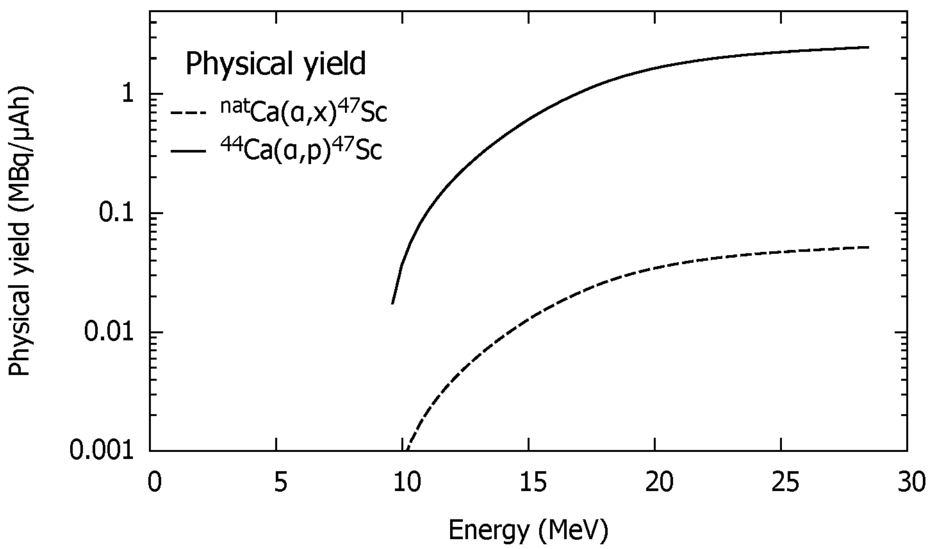


Fig. 8. Physical yields of $^{47}$Sc in the alpha-particle-induced reactions on $^{nat}$Ca and $^{44}$Ca.

## 4. Summary

We measured the activation cross sections of the alpha-particle-induced reactions on natural calcium. The experiment was performed at the RIKEN AVF cyclotron using the stacked-foil activation technique and high-resolution gamma-ray spectrometry. The production cross sections of $^{47,46,44m,44g,43}Sc$ and $^{47}Ca$ using $CaF_2$ target material were measured and converted to those on natural calcium. The derived cross sections are compared with the literature data and the model based theoretically calculated values of the TENDL-2019 library. Physical yields of $^{47}Sc$ via the alpha-particle-induced reactions on $^{nat}Ca$ and $^{44}Ca$ were deduced. The experimental result is expected to contribute to research and development of nuclear medicine using the promising therapeutic radionuclide $^{47}Sc$.

## Acknowledgement

This work was carried out at RI Beam Factory operated by RIKEN Nishina Center and CNS, University of Tokyo, Japan. This work was supported by Japan-Hungary Research Cooperative Program between JSPS and HUS, Grant number JPJSBP120193808 and NKM-43/2019.

## Declarations of interest

None

## Reference

[1] I.F. Chaple, S.E. Lapi, Production and Use of the First-Row Transition Metal PET Radionuclides $^{43,44}Sc$, $^{52}Mn$, and $^{45}Ti$, J. Nucl. Med. 59 (2018) 1655–1659. https://doi.org/10.2967/jnumed.118.213264.

[2] L.F. Mausner, K.L. Kolsky, V. Joshi, S.C. Srivastava, Radionuclide development at BNL for nuclear medicine therapy, Appl. Radiat. Isot. 49 (1998) 285–294. https://doi.org/10.1016/S0969-8043(97)00040-7.

[3] R. Mikolajczak, S. Huclier-Markai, C. Alliot, F. Haddad, D. Szikra, V. Forgacs, P. Garnuszek, Production of scandium radionuclides for theranostic applications: towards standardization of quality requirements, EJNMMI Radiopharm. Chem. 6 (2021) 19. https://doi.org/10.1186/s41181-021-00131-2.

[4] J. Meija, T.B. Coplen, M. Berglund, W.A. Brand, P. De Bièvre, M. Gröning, N.E. Holden, J. Irrgeher, R.D. Loss, T. Walczyk, T. Prohaska, Isotopic compositions of the elements 2013 (IUPAC Technical Report), Pure Appl. Chem. 88 (2016) 293–306. https://doi.org/10.1515/pac-2015-0503.

[5] V. Levkovskij, H. Schopper, Middle mass nuclides (A=40-100) activation cross sections by medium energy (E=10-50) protons and α-particles, 1991.

[6] N. Otuka, E. Dupont, V. Semkova, B. Pritychenko, A.I. Blokhin, M. Aikawa, S. Babykina, M. Bossant, G. Chen, S. Dunaeva, R.A. Forrest, T. Fukahori, N. Furutachi, S. Ganesan, Z. Ge, O.O. Gritzay, M. Herman, S. Hlavač, K. Kato, B. Lalremruata, Y.O. Lee, A. Makinaga, K. Matsumoto, M. Mikhaylyukova, G. Pikulina, V.G. Pronyaev, A. Saxena, O. Schwerer, S.P. Simakov, N. Soppera, R. Suzuki, S. Takács, X. Tao, S. Taova, F. Tárkányi, V. V. Varlamov, J. Wang, S.C. Yang, V. Zerkin, Y.

Zhuang, Towards a More complete and accurate experimental nuclear reaction data library (EXFOR): International collaboration between nuclear reaction data centres (NRDC), Nucl. Data Sheets. 120 (2014) 272–276. https://doi.org/10.1016/j.nds.2014.07.065.

[7] T. Watanabe, M. Fujimaki, N. Fukunishi, H. Imao, O. Kamigaito, M. Kase, M. Komiyama, N. Sakamoto, K. Suda, M. Wakasugi, K. Yamada, Beam energy and longitudinal beam profile measurement system at the RIBF, in: Proc. 5th Int. Part. Accel. Conf. (IPAC 2014), 2014: pp. 3566–3568.

[8] J.F. Ziegler, J.P. Biersack, M.D. Ziegler, SRIM: the Stopping and Range of Ions in Matter, (2008). http://www.srim.org.

[9] National Nuclear Data Center, Nuclear structure and decay data on-line library, Nudat 2.8, (2019). http://www.nndc.bnl.gov/nudat2/.

[10] International Atomic Energy Agency, LiveChart of Nuclides, (2009). https://www-nds.iaea.org/livechart/.

[11] S.Y.F. Chu, L.P. Ekström, R.B. Firestone, The Lund/LBNL Nuclear Data Search, (1999). http://nucleardata.nuclear.lu.se/toi/.

[12] B. Pritychenko, A. Sonzogni, Q-value Calculator (QCalc), (2003). http://www.nndc.bnl.gov/qcalc/.

[13] A. Hermanne, A. V. Ignatyuk, R. Capote, B. V. Carlson, J.W. Engle, M.A. Kellett, T. Kibédi, G. Kim, F.G. Kondev, M. Hussain, O. Lebeda, A. Luca, Y. Nagai, H. Naik, A.L. Nichols, F.M. Nortier, S. V. Suryanarayana, S. Takács, F.T. Tárkányi, M. Verpelli, Reference Cross Sections for Charged-particle Monitor Reactions, Nucl. Data Sheets. 148 (2018) 338–382. https://doi.org/10.1016/j.nds.2018.02.009.

[14] M. Alabyad, G.Y. Mohamed, H.E. Hassan, S. Takács, F. Ditrói, Experimental measurements and theoretical calculations for proton, deuteron and α-particle induced nuclear reactions on calcium: special relevance to the production of $^{43,44}Sc$, J. Radioanal. Nucl. Chem. 316 (2018) 119–128. https://doi.org/10.1007/s10967-018-5733-4.

[15] A.J. Howard, H.B. Jensen, M. Rios, W.A. Fowler, B.A. Zimmerman, Measurement and theoretical analysis of some reaction rates of interest in silicon burning, Astrophys. J. 188 (1974) 131–139.

[16] A.J. Koning, D. Rochman, J. Sublet, N. Dzysiuk, M. Fleming, S. van der Marck, TENDL: Complete Nuclear Data Library for Innovative Nuclear Science and Technology, Nucl. Data Sheets. 155 (2019) 1–55. https://doi.org/10.1016/j.nds.2019.01.002.

[17] N. Otuka, S. Takács, Definitions of radioisotope thick target yields, Radiochim. Acta. 103 (2015) 1–6. https://doi.org/10.1515/ract-2013-2234.